# An X-ray Survey of Galaxies in Pairs

Mark Henriksen and Sarah Cousineau

Physics Department, University of North Dakota, Grand Forks, ND 58202-7129

## **ABSTRACT**

Results are reported from the first survey of X-ray emission from galaxies in pairs. The sample consists of fifty-two pairs of galaxies from the Catalog of Paired Galaxies (CPG) Karachentsev (1972) whose coordinates overlap ROSAT Position Sensitive Proportional Counter (PSPC) pointed observations. The mean observed  $\log l_x$  for early-type pairs is  $41.35\pm0.21$  while the mean log  $l_x$  predicted using the  $l_x$ - $l_b$  relationship for isolated early-type galaxies is  $42.10\pm0.19$ . With 95% confidence, the galaxies in pairs are underluminous in the X-ray, compared to isolated galaxies, for the same  $l_b$ . A significant fraction of the mixed pair sample also appear similarly underluminous. A spatial analysis shows that the X-ray emission from pairs of both types typically has an extent of  $\sim 10$  - 50 kpc, much smaller than group intergalactic medium and thus likely originates from the galaxies. CPG 564, the most X-ray luminous early-type pair,  $4.7 \times 10^{42}$  ergs sec<sup>-1</sup>, is an exception. The extent of it's X-ray emission, >169 kpc, and HWHM, ~80 kpc, is comparable to that expected from an intergalactic medium. The sample shows only a weak correlation,  $\sim 81\%$  confidence, between  $l_x$  and  $l_b$ , presumably due to variations in gas content within the galaxies. No correlation between  $l_x$  and the pair velocity difference ( $\Delta v$ ), separation  $\Delta r$ , or far-infrared luminosity  $(l_{fir})$  is found though the detection rate is low, 22%.

Subject headings: clusters: galaxies: paired galaxies: groups: interacting

galaxies: X-ray Surveys

#### Introduction

Studies of paired galaxies in the radio, infrared, and optical provide important details regarding the role of interactions and mergers in the evolution of galaxies. Evidence of interaction is inferred from excess emission in the far-infrared (FIR) and optical relative to isolated galaxies which indicates an increased level of star formation from the interaction (Bushouse 1987). While these data provide a description of the star formation history of the galaxies, X-ray studies address the fate of gas heated by the large energy input from stellar evolution, such as the formation of a superwind (Heckman, Armus, and Miley 1990). Comparisons of the X-ray and optical luminosity of paired with isolated galaxies provides important details of the connection between star formation and hot gas. Studies of the hot, X-ray emitting gas content of interacting galaxies also has important implications for the enrichment of the intracluster and intergalactic medium. Recent studies of cluster abundances indicate that the enrichment of the ICM has changed little since  $z\sim0.3$  suggest that enrichment must have occurred in protogalaxies rather than during cluster evolution (Mushotzky and Loewenstein 1997). Though local systems are studied here, the results pertaining to the fate of hot gas in paired, interacting galaxies could be applied equally well to protogalactic pairs within clusters.

The X-ray observations are also in a unique position to address the connection between pairs and groups of galaxies. Groups typically have a hot intergalactic medium. If mixedand early-type pair morphologies were merger remnants of groups, then they would retain the hot intergalactic medium of the group, being characterized by an extended X-ray component of >200 kpc, as is typical of groups (Mulchaey et al. 1996). In addition, the total X-ray luminosity of compact groups is higher than that expected from the galaxies themselves (Ponman and Bourner 1997). Detection of the fossil intergalactic medium would make a strong argument that mergers take place within groups.

In this paper, we present the characteristics of the sample and details on the data analysis in section 2. In section 3 we present the results of correlation tests on the entire sample (3.1) and comparisons of the X-ray emission of paired versus isolated galaxies for spiral pairs (3.2), early-type pairs (3.3), and mixed pairs (3.4). In section 4, results of the spatial analysis are presented. In section 5, the results are summarized. A value of 50 km sec<sup>-1</sup> Mpc<sup>-1</sup> is used for all calculated quantities.

## Data Analysis

We have checked the ROSAT PSPC pointed data archives for serendipitous occurrences of over six hundred pairs of galaxies from the optically selected Catalog of Paired Galaxies (CPG) by Karachentsev (1972). Fiftyeight pair positions overlap PSPC pointings. The PSPC is the best instrument to use for this survey because of its larger field of view and greater sensitivity when compared to other available instruments such as the ROSAT high resolution imager or the EIN-STEIN imaging proportional counter (IPC). The pointed observations, while not providing all-sky coverage, have the advantage of much longer exposure times than those of the ROSAT all-sky survey (RASS),  $\sim 550$  seconds, which is necessary since most of these

sources are below the flux limit of the RASS,  $\sim 4 \times 10^{-13}$ ergs cm $^{-2}$  sec $^{-1}$ . Using ROSAT for a survey

of optically selected groups, Mahdavi et al. (1997) found that only seven out of thirtytwo objects are detected on RASS fields of which three are intrinsically much brighter Abell clusters. We detect 11 out of 49 pairs, excluding AGN, at  $> 3\sigma$ . The range in Xray luminosity of groups in their survey exceeds more than 50% of the pairs so that our higher detection rate must be attributed to the longer pointed observations. For a velocity of 6000 km sec<sup>-1</sup>, typical of the paired galaxies, the minimum measurable luminosity with RASS would be  $\sim 3 \times 10^{41}$  ergs sec<sup>-1</sup>. Thus, using the correlations found in this paper, we could expect to detect only the Xray brightest pairs, typically those containing Seyfert galaxies, which are not suitable for study of the hot gas content.

We excluded pairs with have high velocity difference and are therefore chance alignments: CPG 391 ( $>4000 \text{ km s}^{-1}$ ), CPG 321  $(>500 \text{ km s}^{-1})$ , and CPG 166 (>2000 km) $s^{-1}$ )). Pairs in galaxy clusters were also eliminated since they are contaminated by the intracluster medium: CPG 588 (in A2634), CPG 464 (in A2063), CPG 361 (in Coma). CPG 353 is in the outskirts of the Virgo cluster where the contribution from the intracluster medium is negligible and it is included in the sample. The best fit temperature for CPG 353 is 0.82 keV, more typical of emission associated with galaxy than cluster. Since we are addressing the nature of the hot gas content in galaxy pairs, those with AGN were eliminated: CPG 510, CPG 419, CPG 238. CPG 234 also has an extended component (2.3' in extent or 40 kpc) as well as an AGN (section 4) and is included in the analysis. The three pairs with AGN are included in the data Tables and shown in the figures but are not included in any analysis.

Four of the detected pairs were *ROSAT* targets: 125, 218, 278, and 353. Two are spiral pairs and two are mixed-type pairs (CPG 278 and CPG 353). Therefore, the collection of 8 early-type pairs contains only serendipitous observations and represents the unbiased X-ray characteristics of the sample.

Each galaxy pair was first located on the Digitized Sky Survey (DSS) to check the accuracy of the CPG positions. The right ascension and declination given in Tables 1-3 have been modified for some pairs to reflect more accurate coordinates obtained from the DSS than in the CPG. The region size of the image used to measure the X-ray emission was chosen with consideration of the nominal extent of possible extended X-ray emission associated with the galaxies themselves including plumes (Dahlem et al. 1996; Fabbiano 1988), halos (Trinchieri and Fabbiano 1985; Forman, Jones, and Tucker 1985) or the nominal core radius of intergalactic emission from a fossil group using NGC 2300 as a prototype (Davis et al. 1996). It is important to use a fixed, distance-independent sized region for all pairs. This region is a circle with radius equal to the pair separation (in kpc) plus twice the nominal galaxy radius,  $\sim 50$  kpc. In most cases, the emission from either galaxy and from an intergalactic medium would be included within this region. Contaminating point sources were removed when necessary. For wider pair separations or especially difficult locations on the image, a circular region of radius 50 kpc centered on the coordinates of the optically brightest galaxy was used. The size and location of each source region is given in Table 4. Standard PSPC analysis procedures for extended sources, including background subtraction, vignetting and exposure map corrections (Table 4), and charged particle elimination, were followed as outlined in Snowden et al. (1994) to analyze the source regions using routines which are part of the imaging and spectral analysis package in PROS version 2.4 (Deponte, J. et al. 1995).

Signal-to-noise ratios are given in Table 4. The detection threshold is  $3\sigma$  or higher significance. For those source regions with count rates below the detection threshold, an upperlimit is calculated equal to  $3\sigma$ . Spectra for all detected objects were modeled using XSPEC version 9.0 (Arnaud 1996) to obtain the flux. The model consists of a Raymond and Smith plasma code (1977) with absorption cross sections (Morrison and McCammon 1983) using galactic column densities at the source positions (Stark 1992) (values given in Table 4), and solar abundance ratios (Anders and Grevesse 1989). The data was grouped to contain at least twenty counts in each bin to increase the reliability of the results obtained from a chi-square fit (Nousek and Shue 1989). The best-fit plasma temperatures and 90% confidence range from the spectral analysis are given in Table 5.

Upperlimts are converted to fluxes using a Raymond and Smith model convolved with the PSPC response matrix assuming solar abundance and a temperature of 1 keV for early-type and mixed pairs (Kim, Fabbiano, and Trinchieri 1992), for which the X-ray emission is generally dominated by the elliptical galaxy, and 5 keV for spiral pairs (Kim, Fabbiano, and Trinchieri 1992). ROSAT and Advanced Satellite for Astrophysics and Cosmology (ASCA) spectra of spiral galaxies show a soft component in addition to the hard component which dominates the EINSTEIN spectra (see references in section 3) in general agreement with the best-fit values reported in

Table 5 for spiral pairs. In the most extreme case, using a temperature of  $\sim 0.4$  keV from ROSAT spectra of starburst galaxies rather than the nominal temperature would increase the luminosities in Tables 1-3 by a factor of only  $\sim 1.3$ . Since the upperlimits for the spiral pairs are not very constraining in the correlations, the exact temperature used to convert the upperlimits is not critical. The distance is derived from the average of the galaxy pair velocities and used in the luminosity calculation.

X-ray, optical, and FIR luminosities and basic data are shown in Table 1-3 for spiral, early-type, and mixed pairs, respectively. The content of the tables are the following: column (1) is the pair number in the CPG, column (2) is the galaxy classification from NASA/IPAC Extragalactic Database (NED), column (3) and (4) are the RA and DEC in J2000 coordinates, column (5) is the separation of galaxies in minutes of arc, column (6) is the galaxy recessional velocity in  $km sec^{-1}$ , column (7) is the blue luminosity in units of  $10^{43} \text{ ergs sec}^{-1}$ , column (8) is the background subtracted X-ray count rate in counts sec<sup>-1</sup>. column (9) is the  $1\sigma$  error in counts sec<sup>-1</sup>, column (10) is the X-ray luminosity in the 0.25-2 keV band in units of  $10^{41}$  ergs sec<sup>-1</sup>, column (11) is  $l_{FIR}$ . Data in columns (1,3-7) are based on information from Karachentsev (1972). A Hubble constant of 50 km  $sec^{-1}$  $\mathrm{Mpc^{-1}}$  is used to calculate the luminosities. Column 11 is calculated from fluxes obtained from the Catalogue of Galaxies and Quasars Observed in the IRAS Survey, Version 2.1 as well as the Point Source Catalog and the Faint Source Catalog. The FIR sources occur within a 25 kpc search radius centered on each of the galaxy positions.

Table 4 contains supplemental information

to that in Tables 1-3. The content of the tables are the following: column (1) is the pair number in the CPG, column (2) is the PSPC sequence number, column (3) is the size of the source region in arc min, column (4) is the distance of the analyzed region from the center of the image in arcmin, column (5) is the exposure time, column (6) is the signal-to-noise/3, column (7) is the exposure map correction which includes vignetting and correction for the instrument supports, column (8) is the hydrogen column density, column (9) are galaxy UGC, NGC, IC, and CGCG designations of the galaxies in Tables 1-3.

#### 3. Results

### 3.1. Correlations

Normal galaxies all show a correlation between the optical and X-ray luminosity. These correlations allow linking the stellar sources to the amount of hot gas, both stellar and diffuse, thus providing clues to the origin of the X-ray emission. Correlation tests were performed on the subsample of pairs, which included all galaxy types, using  $l_x$  as the dependent variable and the physical quantities:  $l_b$ ,  $l_{FIR}$ ,  $\Delta r$ , and  $\Delta v$  as independent variables.

The  $l_x$ - $l_b$  correlation and other correlation tests were performed using ASURV Rev. 1.2 (LaValley, Isobe, and Feigelson 1992) which implements the methods described in Isobe, Feigelson, and Nelson (1986). Table 6 summarizes the results and has the following column headings and uses the abbreviations which are given in parentheses. Column (1) (labeled DV) is the dependent variable in the bivariate correlation tests. Column (2) (labeled IV) is the independent variable. Column (3) (labeled DET/TOT) is the number of detections and total number of observations used in the

correlation test, Column (4) (labeled GKT) is the probability of a correlation using the Generalized Kendall's Tau. Columns (5-8) are the slope and intercept, with associated errors, from a linear regression analysis using the EM algorithm.

The mean values and variances given in Table 7 are obtained using the non-parametric Kaplan-Meier estimator (Babu and Feigelson 1996). Upperlimits are included in both the paired and isolated galaxy samples. This approach is valid as long as censoring in the sample is random. Visual inspection of the various samples shows the condition of random censoring is met.

The first variables tested were  $l_x$  and  $l_b$ ; the data are shown in Figure 1. The range in  $l_b$  is narrow compared to normal galaxies, a factor of less than 100, and very high, with a mean value  $\sim 10^{44}$  ergs sec<sup>-1</sup>. The range in log  $(l_x)$  is much larger, a factor of  $\sim 10^4$ , and the mean is lower, 40.86 (see table 7). There is a general linear trend between log  $l_x$  and log  $l_b$ . However, the scatter is significant at all luminosities and increases at higher  $l_b$ . The figure also shows that the  $l_x$ - $l_b$  locus is very different for each pair type. Even though there is a weak correlation present, 81%, it is not very tight as is apparent in the large error in the slope.

Strong FIR emission is an indicator of active star formation since interacting galaxies show a high  $1_{FIR}/l_b$ . Close pairs of galaxies with spirals are generally stronger FIR emitters (Xu and Sulentic 1991) implying that they are interacting and should be emitting X-rays associated with massive stars, X-ray binaries, and interstellar gas heated by Type II supernovae. Thirty-six of the spiral pairs and mixed pairs were detected in the FIR but none of the early-type pairs were detected.

Figure 2 shows  $l_{FIR}$  and  $l_x$ . The quantity  $l_{FIR}$ , is calculated from the cataloged FIR flux:

 $Log(F_{FIR} = Log(1.26 \times (F60 + F100)), where F60 = 2.58 \times 10^{-14} \times F_{\nu}(60\mu) \text{ and } F100 = 1.00 \times 10^{-14} \times F_{\nu}(100\mu).$  The fluxes at  $60\mu$  and  $100\mu$  are in Janskys.

We ran correlation tests between  $l_x$ - $l_{FIR}$  and  $l_x$ - $\Delta r$  for the pair samples which have 36 and 49 pairs, respectively. The correlation test results are shown in Table 6; no correlation is present in either instance.

Figure 3 shows X-ray luminosity versus galaxy separation. Though the eye sees a trend of decreasing X-ray luminosity with decreasing separation, they are only weakly correlated (69%).

## 3.2. Spiral Galaxies

Twenty-five pairs of spiral galaxies are analyzed. The X-ray luminosities range from  $< 2.6 \times 10^{40} \text{ to } 10^{42} \text{ ergs sec}^{-1}$ . The  $l_x, l_b$  for pairs is shown in Figure 4 along with  $l_x, l_b$  for a sample of normal spiral galaxies taken from the sample of galaxies observed with EIN-STEIN (Fabbiano, Gioia, and Trinchieri 1988; Trinchieri and Fabbiano 1985). The data are shown in the 0.5 - 3 keV band. Galaxies classified as T=0.10 (very early type or irregular) were removed to get a representative sample of normal spirals. The pairs are converted from the ROSAT band using the canonical spectrum discussed in section 2 to derive luminosities. A value of  $H_0 = 50 \text{ km sec}^{-1}$  $\mathrm{Mpc}^{-1}$  is used in both samples.  $\mathrm{L}_x$  is linearly correlated with  $l_b$  on a log-log scale for the normal galaxy sample, > 99.9\% confidence. We found the mean  $\log(l_x)$  of the paired spirals to be  $40.82 \pm 0.11 \text{ ergs sec}^{-1}$ , higher than the mean value,  $40.06 \pm 0.06 \text{ ergs sec}^{-1}$ , predicted using the  $l_x$ - $l_b$  relationship for isolated spirals observed with EINSTEIN.

Peace and Sansom (1996) analyzed approximately 20 normal spiral galaxies observed with the PSPC. The galaxies in their sample have  $m_B < 13$  and PSPC exposures > 13,000 seconds. They found a mean luminosity of  $\sim 10^{40}$ . This mean is higher than that found for the entire sample observed with EINSTEIN but similar to the value reported above for the subsample of optically bright galaxies. Using hardness ratios, these authors found that the PSPC spectra are consistent with a temperature of 0.85 keV and a range of 0.17 - 3.72 keV, suggesting a softer component may also be present in addition to the >3 KeV hard component (Kim, Fabbiano, and Trinchieri 1992). ASCA observations of the spiral galaxy, NGC 2903 (Mizuno et al. 1996), also show a hard,  $\sim 5 \text{ keV}$  component and a soft  $\sim 0.4 \text{ keV}$  component similar to the spectra they find for the starburst galaxies M82 and NGC 253. We performed a spectral analysis of all of the detected pairs. For most of the spiral galaxies, the data only provide lower limits to the temperature when fitting a Raymond and Smith model (see Table 5). Only for the spiral pair CPG 218, consisting of M81 and M82, is the 90\% temperature range narrow, 0.7 - 1.1 keV. The best-fit temperatures are consistent with a softer X-ray component dominating the ROSAT emission as compared with EINSTEIN. Thus, comparing to the sample in Peace and Sansom, the mean for spiral pairs,  $\log l_x = 40.82$  is significantly higher.

Similar conclusions resulted from a comparison of *EINSTEIN* observations of a subsample of normal galaxies with a sample of peculiar, blue galaxies. The sample of irregular galaxies had several galaxies with much higher  $l_x/l_b$  than the normal galaxies (Fab-

biano, Trinchieri, and MACDonald 1984). The irregular galaxies were chosen primarily for their blue color and in most cases display a disturbed morphology (Fabbiano, Feigelson, and Zamorani 1982).

## 3.3. Early-Type Galaxy Pairs

Eight early-type galaxy pairs are analyzed of which 3 are detected with higher than  $3\sigma$ significance. The sample of normal early-type galaxies observed with EINSTEIN (Eskridge, Fabbiano, and Kim 1995a) is shown in Figure 5 with the best fit line for comparison. A value of 50 km  $\sec^{-1} \mathrm{Mpc^{-1}}$  for the Hubble Constant was used in both samples and the pair luminosities were converted to the energy band of the normal galaxies, 0.2 - 4 keV, using the canonical spectrum described in section 2. These authors found that the sample is best characterized by two linear relations and those with  $\log l_x > 40.5$  have a best fit line with a steeper slope,  $\simeq 2$ . This attributed to X-ray emission from low luminosity normal galaxies being dominated by low mass X-ray binaries while the high  $l_x$  have a dominant contribution from hot gas. All of the pairs have  $l_x > 40.5$ ; they are X-ray bright and fall into the latter category. Compared to the normal galaxies, the early-type pairs appear underluminous in X-rays for their  $l_b$ . We compare the observed  $l_x$  for pairs with the sum of the predicted  $l_x$  for each galaxy. The predicted  $l_x$  is calculated from the  $l_b$ for the galaxies individually, then added to get the predicted  $l_x$  for the pair. The relationship reported by Eskridge, Fabbiano, and Kim (1995a) for the brightest ellipticals,  $l_x \sim$  $l_b^2$ , is used for the predicted values. Figure 6 shows that the observed values systematically fall below the predicted values, except in the case of the detected pair, CPG 564, for which we report evidence of an intergalactic medium (section 4). The mean predicted log  $l_x$  is  $42.10\pm0.19$ :  $2\sigma$ , 95% confidence, higher than the mean observed value of the pairs,  $41.35\pm0.21$ . If CPG 564 is excluded, the mean observed log  $l_x$  decreases to  $41.16\pm0.12$  and the difference increases to  $3\sigma$ .

The blue magnitudes from Karachentsev (1972) are isophotal and extend to the B=26mag./sq. arcsec isophote. This is one magnitude fainter than the limiting value in RC2 which was used in the comparison sample of early type galaxie in Eskridge et al. (which is based on Fabbiano et al. (1992)). The NED data base was used to obtain the RC3 magnititudes for the brightest galaxy in the 8 pairs. The magnitudes from the CPG and RC3 are both corrected for extinction in the Milky Way. The CPG pairs are additionally corrected for internal extinction based on galaxy type and inclination. The values are listed for comparison with the CPG magnitude given first: CPG 18(14.78,14.60), CPG 90(15.39,15.7), CPG 99(12.91,12.61), CPG 175 (13.21,12.12), CPG 320(14.49,14.9), CPG 367(14.52,13.64), CPG 564(14.63, 14.32), CPG 574(13.98,13.63). The RC3 values for CPG 18, CPG 90, and CPG 320 are not corrected for extinction and CPG 90 and CPG 320 are a little high. For all of the other pairs the RC3 magnitude is slightly lower; generally all of the pairs agree within the published RC3 error. The trend reported in this paper, that early- and mixed-type pairs have a lower  $l_x$ for their  $l_b$  (based on the CPG) can not be explained as a systematic overestimate of the l<sub>b</sub> from CPG relative the RC3, on which the camparison sample is based. On both figures 5 and 6, use of the RC3 magnitudes for the paired galaxies would generally shift the pairs to the right, making the underluminosity more evident.

The process of disk galaxy merger can give a blue luminosity much higher than is typical of even the brightest isolated galaxies (Caon et al. 1994). High  $l_b$  galaxies occupy a region of the fundamental plane consistent with mergers of systems which are generally less gaseous and more stellar (Bender et al. 1992). Thus, those galaxies which have a high  $l_b$  are associated with interaction and in some cases, The very high  $l_b$  early-type pairs are also characterized by a low X-ray luminosity similar to NGC 4125 and NGC 3610. These galaxies also have low 0.1 - 2 keV Xray luminosities and have plumes of emission suggesting the later stages of a merger (Fabbiano and Schweizer 1995). The prototype for the pairs is the close elliptical pair, CPG 99, found to show evidence of tidal interaction in the form of a U-shaped velocity dispersion (Borne and Hoessel 1988; Bonfanti et al. 1995). In addition, the galaxy NGC 1587, which is part of the pair was argued to be a merger remnant on the basis of an angular momentum which could not be attributed to the present interaction. The CPG 99 pair is detected at  $>3\sigma$  and has a low  $l_x$ , < $10^{41} \text{ ergs sec}^{-1}$ , for it's  $l_b$ ,  $\sim 2 \times 10^{44} \text{ ergs sec}^{-1}$ . The early-type pairs typically have low  $l_x$  and may show evidence of being merger remnants as well as interaction with their companion. The NGC4782/4783 pair (Colina and Borne 1995) also shows a low integrated X-ray luminosity,  $\sim 2 \times 10^{41}$  ergs sec<sup>-1</sup>, typical of the underluminous pairs found here. High resolution studies of the 4782/4783 system show multiple X-ray components resulting from the interaction and merger of the two galaxies which includes tidal heating and shock heating from the collision. This detailed study supports the hypothesis that in the underlu-

minous pairs the X-ray emission is directly associated with the interaction/merger. The spatial analysis presented in section 4 contained CPG 99 and CPG 564. CPG 99 is underluminous by nearly a factor of 10, the least X-ray luminous detection. The spatial analysis shows it has a very small radial extent of  $\sim$ 47 kpc and small core radius when compared to similar parameters for groups. For example, the NGC 2300 group has a radial extent of >250 kpc. In contrast, the only pair with a luminosity over that predicted, CPG 564, has X-ray emission extending to >169 kpc, which is likely intergalactic. The gas temperature is 1.03 + 0.9 / -0.26 keV, similar to that found for groups. If the underluminous earlytype galaxy pairs such as CPG 99 are merger remnants, then they must have formed out of spiral pairs with no intergalactic medium. Generally, these are the low velocity dispersion groups (Mulchaey et al. 1996). Spectral fits performed on five detected paired galaxies gave significant temperature constraints with best fitting temperatures between 0.20 - 1.26 keV; in all cases the 90% range in temperature excludes a hard component dominating the emission. Thus, the spectrum is dominated by hot gas. ASCA and ROSAT spectra of normal elliptical galaxies show both a hard component, with  $l_x$  correlated with  $l_b$  (Matsushita et al. 1994) implying a stellar origin, and a soft component which dominates the emission of bright ellipticals (Fabbiano, Kim, and Trinchieri 1994; Kim et al. 1996). The soft component originates in hot gas with the most X-ray luminous normal ellipticals being consistent in their  $l_x$ - $l_b$  relationship with a steady state cooling flow (Sarazin and Ashe 1989).

The gas dynamics in normal elliptical galaxies fit a somewhat simple picture in which

the temperature of the hot gas component is proportional to the velocity dispersion of the galaxy but is not in energy equipartition with the stellar component implying that the gas is heated and bound by the dark matter dominated gravitational potential (Davis and White 1996; Eskridge, Fabbiano, and Kim 1995b). Studies of several pairs show that they are dynamically complex with U-shaped velocity dispersion profiles, presumably from tidal heating in the outer radii. Analogous to the stars, the gas would also be tidally Tidally triggered dynamical heating as well as that from star formation may be sufficient to overcome the binding gravitational potential of the galaxy. This would account for the paired galaxies being among the least luminous of those normal early-type galaxies which are classified as X-ray luminous and dominated by hot gas. Simple calculations by Mathews and Brighenti (1997) suggest that a factor of  $\sim 10$  underluminous interacting early-type galaxies must be recent merger/interactions,  $\sim 10^9$  years, due to replenishment of the interstellar gas by stellar mass loss. This would make gas deficiency an unlikely explanation for a large number of low  $l_x/l_b$  galaxies on statistical grounds. Figure 5 indicates that approximately half of the pairs are underluminous by a factor of 10 compared to the best fit linear regression found for normal early-type galaxies. However, paired galaxies are expected to show a higher frequency of recent and ongoing interaction/merger than single galaxies which may represent merger products so that gas lost may not have been fully replenished by stellar mass loss.

Galaxies in early-type pairs show evidence of interaction and merger based on very high blue luminosities and disturbed velocity dis-

persion profiles. They also tend to be deficient in X-rays which, because of their soft spectra indicate a deficiency in hot gas. This may have important consequences for enrichment of the intergalactic medium with metals. One of the ways in which non-isolated galaxies evolve, whether the environment is a pair, group, or cluster may be through interactions with another galaxy. That interaction with a companion appears to destabilize gas within the pair system so that it can not be bound by the galaxies. If the pairs were in a cluster or group environment, the intergalactic medium would be enriched during the merger process since the more massive system would be able to bind the gas. These results would apply equally well to a cluster of protogalaxies in which recent observations of cluster abundances imply the enrichment must occur (Mushotzky and Loewenstein 1997).

#### 3.4. Mixed Type Galaxy Pairs

There are 16 mixed morphology pairs of which 3 are detected at  $>3\sigma$ . Figure 7 shows observed  $l_x$  versus predicted  $l_x$  in the 0.2 - 4 keV band. The predicted values are the sum of the individual values predicted for each galaxy using the  $l_x$  -  $l_b$  appropriate for each galaxy class. There are eight pairs: 2 detections and 6 upper limits, with luminosities below that predicted. Four (2 detections and 2 upperlimits) are significantly underluminous. A spatial analysis of the two detections, CPG 278 and CPG 353 shows emission centered on both galaxies in the case of 278 and on the elliptical in the case of CPG 353. The 90% confidence range in temperature for CPG 278 is 0.31 - 0.57 keV, lower than all of the groups reported in Mulchaey et al. (1996). The temperature of CPG 353 is 0.78 - 0.85 keV; however, both have X-ray emission about a factor

of 10 below that predicted for their  $l_b$ . They are underluminous in the same sense that the early-type pairs are underluminous; they are gas poor galactic systems and lack an additional intergalactic component.

#### 4. Spatial Analysis

Eight detections (excluding those dominated by AGN) are located in an appropriate region of the detector and had sufficient counts for spatial analysis: CPG 234, CPG 239, CPG 278, and CPG 353 (mixed pairs), CPG 99 and CPG 564 (early-type), CPG 125 and CPG 218 (spiral pairs). The PSPC images were flatfielded, corrected for vignetting, and background subtracted prior to further analysis.

Radial profiles were made using the X-ray peak as the center (Figures 8 - 15). These are used to obtain the extent of the X-ray emission. X-ray contours are overlayed on the Digitized Sky Survey image (Figures 16 - 21) to see the relationship between the X-ray emission and the galaxies. The contours are smoothed with a Gaussian of width 22.5 arcsec, chosen to minimize the confusion between close galaxy pairs.

From the radial profiles, the peak surface brightness and HWHM is measured as well as the approximate radial extent. For CPG 125, 218, and 278, the emission is resolved into two distinct components: one centered on each galaxy. There is an entry in Table 8 for each galaxy in these pairs. Intergalactic group X-ray emission is typically fit by a  $\beta$  of 0.5 using the radial profile,  $(1 + (r/r_c)^2)^{-3\beta+0.5}$ . For this profile,  $r_c$  is equal to the HWHM so that the core radii measured by Mulchaey et al. (1996) using this profile can be compared with the HWHM measured for the pairs.

The HWHM of CPG 125 and CPG 218, the spiral pairs is consistent with a point source while for the other 6 pairs the emission is extended. This comparison was made allowing for the broadening PSF of the PSPC with radius. The HWHM for the pairs with extended emission are generally smaller than the core radii of groups. The extent of the gas is much smaller than groups, except in the case of CPG 564. CPG 564 is, in fact, the most luminous early-type pair,  $4.7 \times 10^{42}$  ergs sec<sup>-1</sup> and comparable to the brightest in the survey of isolated galaxies. The extent of it's X-ray emission, >169 kpc, and HWHM,  $\sim 80$  kpc, is comparable to that from an intergalactic medium. However, the X-ray profiles of the other five indicate galactic emission.

The X-ray emission originating from hot gas in early- and mixed-type pairs show they are generally underluminous in X-rays compared to that expected from isolated galaxies. There is also no spatial evidence that these optically selected pairs have intergalactic gas similar to the NGC2300 system. If the early- and mixed-type galaxies formed through mergers, they must have formed from spiral rich groups with little or no intergalactic medium. These are generally groups with a low velocity dispersion (Mulchaey et al. 1996).

#### 5. Conclusions

We have completed the first X-ray survey of optically selected galaxies in pairs using ROSAT pointed observations. An analysis of the hot gas content in early- and mixed-type galaxy pairs indicates that they are generally characterized by a lower  $l_x$  for their  $l_b$  compared to normal galaxies. A spatial analysis indicates that the extent of the X-ray emission is much less than the intergalac-

tic medium of a group and is centered on a galaxy. This is consistent with X-ray emission being galactic in origin. The mean  $l_x$ for early-type pairs is  $2\sigma$ , 95% confidence, lower than the mean predicted if they were isolated galaxies implying that they are gas poor. Mixed pairs show this same trend. The X-ray brightest pair, CPG 564, is an exception to this trend since a spatial and spectral analysis shows its emission is likely intergalactic. These pairs show evidence of interaction and possibly merger in other wavebands. If they have formed through mergers, then the lack of any intergalactic emission could be explained if they formed out of spiral dominated, low velocity dispersion groups. These typically have no intergalactic medium.

The spiral galaxy pair sample has a number of pairs with significantly higher  $l_x/l_b$  than the normal galaxy sample, comparable to the brighter starburst galaxies and less luminous Seyfert galaxies.

X-ray studies of galaxies in pairs are of fundamental importance to understanding the impact of interacting galaxies on galaxy evolution. Enrichment of the intergalactic medium may also be tied to protogalactic interactions and gas loss as reported here for earlyand mixed-type pairs. The relationship between the X-ray emission of pairs and galaxy groups of 3-4 members is also crucial to understanding the dynamical history of the groups and any dependence on morphology. Future detailed studies of individual pairs of each galaxy type which provide spatially and spectrally resolved X-ray components are necessary to discover the detailed interaction history of these interesting objects.

MH and SC gratefully acknowledge support for this project from the National Science

Foundation grant No. AST-9624716. We are thankful to the referee, Trevor Ponman, for critical comments on the manuscript.

#### REFERENCES

- Anders, E., and Grevesse, N., 1989, Geochimica et Cosmochimica Acta 53, 197
- Arnaud, K., 1996, Astronomical Data Analysis Software and Systems V, eds. Jacoby, G., and Barnes, J., ASP Conf. Series, 101, 17
- Babu, G., and Feigelson, E., 1996, Astrostatistics, Chapman and Hall
- Bender, R., Burstein, D., and Faber, S., 1992, ApJ, 399, 462
- Bonfanti, P., Rampazzo, R., Combes, F., Prugniel, P., and Sulentic, J., 1995, Astron. & Astrophys., 297, 28
- Borne, K., Hoessel, J., 1988, ApJ, 330, 51
- Bushouse, H., 1987, ApJ, 320, 49
- Caon, N., Capaccioli, M., D'Onofrio, M., Longo, G., 1994 Astron. & Astrophys., 286, L39
- Colina, L., and Borne, K., 1995, ApJ, 454, L101
- Dahlem, M., Heckman, T., Fabbiano, G., Lehnert, M., Gilmore, D., 1996, ApJ, 461, 724
- Davis, D.S., Mulchaey, J., Mushotzky, R.F., Burstein, D. 1996, ApJ, 460, 601
- Davis, D.S., and White, R.E. III, ApJ, 70, 35

- Deponte, J., Chen, J., Manning, K., Schmodt, D., and Van Stone, D., 1995, Astronomical Data Analysis Software and Systems IV, eds. Shaw, R.A., Payne, H., and Hayes, J., ASP Conf. Series, 77, 410
- Eskridge, P., Fabbiano, G., and Kim, D.-W., 1995, ApJS, 97, 141
- Eskridge, P., Fabbiano, G., and Kim, D.-W., 1995, ApJ, 442, 523
- Fabbiano, G., Feigelson, E. Zamorani, G., 1984, ApJ, 256, 397
- Fabbiano, G., Trinchieri, G., and MacDonald, A., 1984, ApJ, 284, 65
- Fabbiano, G., 1988, ApJ, 330, 672
- Fabbiano, G., Gioia, I.M., Trinchieri, G. 1988, ApJ, 324, 749
- Fabbiano, G., Kim, D.-W., and Trinchieri, G. 1994, ApJ, 429, 94
- Fabbiano, G., and Schweizer, F., 1995, ApJ, 447, 572
- Forman, W., Jones, C., and Tucker, W., 1985, ApJ, 293, 102
- Heckman, T., Armus, L., Miley, G., ApJS, 74, 833
- Isobe, T., Feigelson, E., Nelson, P., 1986, ApJ, 306, 490
- Karachentsev, I., 1972, Comm. Spec. Ap. Obs., USSR, 7, 1 (CPG)
- Kim, D.,-W., Fabbiano, G., Trinchieri, G. 1992, ApJ, 393, 134
- Kim, D.,-W., Fabbiano, G., Matsumoto, H., Koyama, K., and Trinchieri, G. 1996, ApJ, 468, 175

- LaValley, M., Isobe, T., Feigelson, 1992, B.A.A.S. (Software Reports), 24, 839.
- Mathews, W., and Brighenti, F., 1997, The Second Stromolo Symposium: The Nature of Elliptical Galaxies, M. Arnaboldi, G. Da Costa, & P. Saha, ASP Conference Series, 116, 405
- Matsushita, K., et al., 1994, ApJ, 436, L41
- Mizuno T., et al. 1997, X-ray Imaging and Spectroscopy of Cosmic Hot Plasmas, Makino and Matsuda, Universal Academy Press, Inc., 1997, 181
- Morrison, R., and McCammon, D., 1983, ApJ, 270, 119
- Mulchaey, J., Davis, D., Mushotzky, R., and Burstein, D., 1996, ApJ, 456, 80
- Mushotzky, R., and Loewenstein, M., 1997, ApJ, 481, L63
- Nousek, J., and Shue, D., 1989, ApJ, 342, 1207
- Peace, G.A., and Samson, A.E. 1996, MPE Report 263, 387
- Ponman, T., and Bourner, P. 1997, X-ray Imaging and Spectroscopy of Cosmic Hot Plasmas, Makino and Matsuda, Universal Academy Press, Inc., 1997, 149
- Raymond, J., and Smith, B., 1977, ApJS, 35, 419
- Sarazin, C., and Ashe, G., 1989, ApJ, 345, 22
- Snowden, S., McCammon, D., Burrows, D., and Mendenhall, J., 1994, ApJ, 424, 715
- Stark, A., 1992, APJS, 79, 77

- Trinchieri, G., and Fabbiano, G., 1985, ApJ, 296, 447
- de Vaucouleurs, G., de Vaucouleurs, A., Corwin, H., Buta, R., Paturel, G., and Fouque, P., 1991, Third Reference Catalogue of Bright Galaxies (Springer, New York).

Xu, C., and Sulentic, J., 1991, ApJ, 374, 407

This 2-column preprint was prepared with the AAS LATeX macros v4.0.

TABLE 1

DATA FOR SPIRAL GALAXY PAIRS

CPG	Type	RA	Dec	Sep	Vel	$L_b$	$\frac{Cnts}{sec} \times 10^{-2}$	σ	$L_x$	$\text{Log L}_{FIR}$
3	S	00 10 33	28 59 46	1.5	7131	3.41	1.49	1.55	<12.10	44.12
	$\operatorname{Sc}$	$00\ 10\ 26$	$28\ 59\ 14$	-	7307	11.70	-	-	-	-
7	S0?	$00\ 21\ 13$	$30\ 28\ 26$	2.06	4909	2.73	0.27	0.95	< 3.41	-
	SB?	$00\ 21\ 16$	$30\ 30\ 20$	-	4943	2.69	-	-	-	43.29
13	SA(s)ab	$00\ 36\ 52$	$23\ 59\ 29$	0.37	4496	10.76	0.28	0.50	< 1.55	43.82
	SAB pec	$00\ 36\ 52$	$23\ 59\ 05$	-	4674	2.06	-	-	-	-
31	S pec	$01\ 24\ 33$	$03\ 48\ 03$	0.65	2276	5.87	0.77	0.34	< 0.26	44.56
	$\mathbf{S}$	$01\ 24\ 35$	$03\ 47\ 22$	-	2216	2.30	-	-	-	-
125	$\operatorname{pec}$	$07\ 09\ 12$	$20\ 36\ 06$	2.57	5051	11.09	2.40	0.46	3.80	-
	S pec	$07\ 09\ 17$	$20\ 38\ 11$	-	5154	30.10	-	-	-	44.92
136	S?	$07\ 27\ 22$	$19\ 38\ 22$	1.00	9660	16.60	0.47	0.36	< 5.03	44.55
	S?	$07\ 27\ 24$	$19\ 37\ 27$	-	9821	14.80	-	-	-	-
137	$\mathbf{S}$	$07\ 36\ 44$	$74\ 26\ 57$	0.46	3918	1.33	1.57	0.37	0.61	43.48
	$\mathbf{S}$	$07\ 36\ 37$	$74\ 26\ 45$	-	3927	1.04	-	-	-	-
140	$\operatorname{Sb}$	$07\ 44\ 07$	$29\ 14\ 57$	0.54	4739	5.03	0.52	0.45	< 1.53	43.69
	$\operatorname{Sa}$	$07\ 44\ 09$	$29\ 14\ 50$	-	4791	5.85	-	-	-	-
161	SAB	$08\ 23\ 33$	$21\ 20\ 15$	0.72	5318	3.03	0.16	0.13	< 3.62	43.05
	$_{ m SB}$	$08\ 23\ 34$	$21\ 20\ 51$	-	5291	2.11	-	-	-	-
163	S?	$08\ 29\ 15$	$55\ 31\ 21$	0.88	7777	6.98	5.61	2.52	< 22.80	44.07
	$\operatorname{Sbc}$	$08\ 29\ 21$	$55\ 29\ 29$	-	7828	9.15	-	-	-	-

Table 1—Continued

CPG	Type	RA	Dec	Sep	Vel	$L_b$	$\frac{Cnts}{sec} \times 10^{-2}$	$\sigma$	$L_x$	$\text{Log L}_{FIR}$
171	S?	08 46 01	12 47 09	1.54	8833	15.08	-0.68	0.97	<11.2	44.18
	S?	$08\ 45\ 55$	$12\ 46\ 57$	-	8788	14.30	-	-	-	-
186	$\operatorname{Sm}$	$09\ 05\ 48$	$25\ 26\ 11$	0.78	2627	0.55	0.54	0.40	< 0.40	43.85
	$\operatorname{Sc}$	$09\ 05\ 48$	$25\ 26\ 11$	-	2553	6.73	_	-	-	43.96
200	$\operatorname{Sb}$	$09\ 25\ 00$	$64\ 33\ 37$	2.01	5137	4.44	-0.91	0.69	< 2.91	-
	$\operatorname{Sb}$	$09\ 25\ 05$	$64\ 31\ 40$	-	5485	3.19	-	_	-	-
204	$_{ m SB}$	$09\ 27\ 45$	$12\ 17\ 15$	0.23	8496	9.05	1.14	0.59	< 5.20	44.19
	$\operatorname{Im}$	$09\ 27\ 44$	$12\ 17\ 14$	-	8546	7.25	-	_	-	
218	I0	$09\ 55\ 51$	$69\ 40\ 26$	39.6	95	0.68	116.80	2.97	0.60	- 44.61
	SA(s)ab	$09\ 55\ 34$	69 04 11	-	388	3.76	-	_	-	-
246	Šá	$10\ 43\ 30$	$12\ 05\ 14$	2.76	7790	10.40	0.43	0.42	< 3.75	-
	$\operatorname{Sc}$	10 43 39	$12\ 03\ 36$	-	7761	8.43	-	_	-	-
258	pair?	$10\ 59\ 05$	$72\ 38\ 00$	0.87	8217	11.05	-0.093	0.38	< 3.83	44.22
	Sa	$10\ 58\ 57$	$72\ 38\ 33$	-	8179	4.52	-	_	-	-
347	SA(rs)bc	$12\ 36\ 32$	$11\ 15\ 28$	1.3	2112	8.54	1.67	0.48	1.1	44.37
	$\widehat{SA(rs)bc}$	$12\ 36\ 37$	$11\ 14\ 20$	-	2158	9.17	-	-	-	-
378	Sb pec	$13\ 30\ 06$	-01 43 17	3.72	4121	10.97	1.29	0.38	1.3	44.09
	SAB(r)c	13 30 11	-01 39 51	-	4055	11.10	-	-	-	-
410	$\widehat{\mathrm{SAc}}$	$14\ 03\ 23$	$09\ 26\ 51$	1.57	5638	11.13	0.28	0.37	< 1.45	44.05
	$\operatorname{Sbc}$	$14\ 03\ 27$	$09\ 27\ 59$	_	5637	8.71	-	-	-	-

Table 1—Continued

CPG	Type	RA	Dec	$\operatorname{Sep}$	Vel	$L_b$	$\frac{Cnts}{sec} \times 10^{-2}$	$\sigma$	$L_x$	$\mathrm{Log}\ \mathrm{L}_{FIR}$
419	Sa pec	14 13 20	-03 08 56	3.82	1954	2.42	32.44	2.31	7.80	-
	SAB(r)	$14\ 13\ 15$	-03 12 27	-	1782	2.11	-	-	-	43.77
422	(R)SB(rs)0/A	$14\ 17\ 03$	$36\ 34\ 17$	0.59	3139	4.92	0.47	0.29	< 4.58	43.31
	SA(s)bc	$14\ 17\ 05$	$36\ 34\ 30$	-	3145	1.68	-		-	_
473	$\operatorname{Sb}$	$15\ 49\ 57$	$20\ 48\ 16$	0.48	10781	16.73	0.13	0.21	< 3.63	44.52
	$\mathbf{S}$	$15\ 49\ 59$	$20\ 48\ 31$	-	10803	12.30	-	-	-	_
534	$\operatorname{Sb}$ pec	$18\ 12\ 56$	$68\ 21\ 45$	0.73	6495	9.10	0.44	0.83	< 0.54	44.85
	$\operatorname{Sa}$	$18\ 12\ 60$	$68\ 21\ 16$	-	6716	11.30	-	-	-	_
557	SBa	$21\ 28\ 58$	$11\ 21\ 58$	0.67	8646	9.37	0.24	0.29	< 3.23	44.05
	$_{ m SB}$	$21\ 28\ 59$	$11\ 22\ 59$	-	8665	8.43	-	-	-	_
566	SB?	$22\ 19\ 28$	$29\ 23\ 45$	0.84	4994	2.98	0.043	0.58	< 2.04	44.63
	S?	$22\ 19\ 30$	$29\ 23\ 14$	-	4768	2.93	-	-	-	-

 $\begin{tabular}{ll} Table 2 \\ Data for Early-type Galaxy Pairs \\ \end{tabular}$ 

CPG	Type	RA	Dec	Sep	Vel	$L_b$	$\frac{Cnts}{sec} \times 10^{-2}$	σ	$L_x$
18	E	00 48 31	01 21 17	0.34	18648	36.30	0.82	0.34	<14.9
	$\mathbf{E}$	$00\ 48\ 30$	$01\ 21\ 12$	-	19003	54.40	-	-	_
90	$\mathbf{E}$	$03\ 25\ 04$	$02\ 53\ 46$	1.07	9487	7.73	0.18	0.16	< 1.65
	$\mathbf{E}$	$03\ 25\ 01$	$02\ 54\ 27$	-	9159	7.08	-	-	-
99	E pec	$04\ 30\ 40$	$00\ 39\ 42$	0.97	3800	12.20	1.25	0.359	0.94
	E pec	$04\ 30\ 44$	$00\ 39\ 52$	-	3495	4.67	-	-	-
175	E1-2	$08\ 49\ 22$	$19\ 04\ 29$	0.56	4206	11.30	2.05	0.64	3.35
	E0 pec	$08\ 49\ 24$	$19\ 04\ 26$	-	3850	3.67	-	-	-
320	$\mathbf{E}$	$12\ 05\ 41$	$01\ 35\ 37$	1.10	5959	5.45	0.064	0.24	< 0.98
	SB(s)0	$12\ 05\ 41$	$01 \ 34 \ 29$	-	5550	4.95	-	-	-
367	S0?	$13\ 14\ 52$	$17\ 13\ 36$	1.28	7087	9.62	-0.80	2.73	< 16.60
	$\mathbf{E}$	$13\ 14\ 57$	$17\ 13\ 33$	-	7012	6.11	-	-	_
564	SA0-	$22\ 14\ 47$	$13\ 50\ 25$	0.59	8212	11.70	6.07	0.76	46.5
	SA0-	$22\ 14\ 45$	$13\ 50\ 45$	-	7964	11.70	-	-	_
574	S0	$22\ 51\ 00$	$31\ 22\ 28$	0.57	6778	14.5	0.48	1.32	< 7.87
	E	$22\ 51\ 04$	31 22 28	-	7216	3.90	-	-	-

 $\begin{array}{c} \text{Table 3} \\ \text{Data for Mixed Galaxy Pairs} \end{array}$ 

CPG	Type	RA	Dec	Sep	Vel	$L_b$	$\frac{Cnts}{sec} \times 10^{-2}$	σ	$L_x$	$\text{Log }(l_{FIR})$
83	RingA	02 55 10	-00 10 41	0.71	8514	37.20	0.17	0.26	< 2.33	45.04
	RingB	$02\ 55\ 12$	-00 11 00	-	8714	23.90	-	-	-	-
116	$\operatorname{Sc}$	$07\ 02\ 31$	$86\ 34\ 47$	1.57	5005	2.00	0.22	0.34	< 1.04	43.75
	$\mathbf{E}$	$07\ 03\ 21$	$86\ 33\ 29$	-	4951	4.16	-	-	-	-
144	E	$07\ 48\ 13$	$28\ 13\ 30$	0.54	8107	9.99	0.64	0.54	< 4.36	-
	$\operatorname{Sa}$	$07\ 48\ 11$	$28\ 13\ 50$	-	8210	4.69	-	-	-	44.66
234	E2	$10\ 23\ 27$	$19\ 53\ 50$	2.35	1168	1.00	26.29	0.45	11.	=
	SAB(s) pec	$10\ 23\ 31$	$19\ 51\ 54$	-	1063	2.09	-	-	-	43.39
238	$\mathbf{E}$	$10\ 34\ 30$	$39\ 36\ 54$	2.34	12862	13.70	331.70	3.17	867.	=
	compact	$10\ 34\ 39$	$39\ 38\ 29$	-	12951	13.90	-	-	-	=
239	E?	$10\ 36\ 21$	$58\ 37\ 11$	3.92	8216	15.30	1.82	0.92	< 7.65	=
	SABbc	$10\ 36\ 26$	$58\ 33\ 22$	-	8252	9.98	-	-	-	=
243	S0	$10\ 40\ 45$	$39\ 04\ 25$	1.08	9015	3.66	0.19	0.19	< 1.91	=
	S	$10\ 40\ 40$	$39\ 03\ 57$	-	8914	11.50	-	-	-	44.29
260	E?	$10\ 59\ 59$	$50\ 03\ 24$	2.72	7235	9.66	0.44	0.39	< 2.54	=
	S?	$10\ 59\ 53$	$50\ 00\ 53$	-	7434	13.90	-	-	-	=
278	SA(s)	$11\ 16\ 55$	$18\ 03\ 04$	5.96	841	7.44	8.52	0.71	0.45	=
	$\mathbf{E}$	$11\ 16\ 59$	$18\ 08\ 54$	-	1118	3.40	-	-	-	
339	SB0?	$12\ 28\ 13$	$13\ 53\ 56$	1.57	7041	8.42	-1.94	0.71	< 4.44	-
	$\operatorname{Scd}$	$12\ 28\ 07$	$13\ 54\ 43$	-	7269	10.80	-	-	-	43.72

Table 3—Continued

CPG	Type	RA	Dec	Sep	Vel	$L_b$	$\frac{Cnts}{sec} \times 10^{-2}$	$\sigma$	$L_x$	$\text{Log }(l_{FIR})$
345	S0/a	12 32 48	63 56 22	4.02	2591	5.46	0.055	0.32	< 0.32	-
	SB(s)dm	$12\ 32\ 34$	$63\ 52\ 38$	-	3073	2.02	-	_	-	43.00
353	m E2	$12\ 43\ 40$	$11\ 33\ 07$	2.57	1170	20.30	43.44	1.00	3.1	-
	SAB(rs)c	$12\ 43\ 33$	$11\ 34\ 57$	-	1382	3.83	-	_	-	43.50
402	SO	$13\ 55\ 59$	$17\ 29\ 57$	0.73	6202	2.10	0.40	0.22	< 1.11	-
	$\mathbf{S}$	$13\ 56\ 00$	$17\ 30\ 40$	-	6528	4.69	-	_	-	43.89
494	$\mathbf{E}$	$16\ 17\ 36$	$46\ 04\ 57$	1.15	6102	2.25	-0.68	1.13	< 5.00	-
	$\operatorname{Sab}$	$16\ 17\ 31$	$46\ 05\ 30$	-	5919	4.73	-	_	-	44.21
508	E0	$17\ 19\ 14$	$48\ 58\ 50$	3.79	7488	5.69	0.65	0.32	< 2.14	-
	$\operatorname{Sb}$	$17\ 19\ 21$	$49\ 02\ 50$	-	7420	8.30	-	-	-	43.92
510	$\mathbf{E}$	$17\ 22\ 39$	$30\ 52\ 11$	0.77	13694	20.50	33.80	2.69	315.	-
	SAB(r)a	$17\ 22\ 40$	$30\ 52\ 52$	-	13215	20.70	-	_		-
530	$\mathbf{E}$	$18\ 10\ 58$	$31\ 06\ 56$	9.27	7227	14.50	-0.50	0.72	< 4.60	-
	$\operatorname{Scd}$	$18\ 10\ 27$	$31\ 00\ 11$	-	7238	8.19	-	_	-	43.91
548	E+pec	$20\ 47\ 24$	$00\ 18\ 02$	1.76	4032	5.99	0.95	0.47	< 1.03	-
	SAB(r)ab	20 47 19	00 19 11	-	4419	15.30	-	-	-	43.53

Table 4
Supplemental Data for All Pairs

(1)	(2)	(3)	(4)	(5)	(6)	(7)	(8)	(9)
3	wp200645	3.5	51.0	2717	0.32	1.67	4.7	N27, U96, C0007.9+2844
7	rp201507n00	4.4	47.0	4849	0.10	1.77	5.8	U95, C0007.9+2843 C0018.6+3011 C0018.7+3014
13	rp800464n00	3.8	3.3	7709	0.19	1.04	3.3	N169, U365, C0034.2+2343
18	rp700377n00	2.9	38.13	10447	0.79	1.41	2.6	N169A,C0034.2+2343 I1559,U496,C0045.9+0105 U496,C0045.9+0105
31	wp701047n00	4.0	0.50	13894	0.75	1.03	2.9	N520,U966,C0122.1+0333
83	rp701403n00	2.3	21.8	11863	0.22	1.63	5.5	N520,U966,C0122.1+0333 N1143,U2388,C0252.6-0023 N1144,U2389,C0252.6-0023
90	rp700099	3.0	33.79	25727	0.39	1.71	8.8	C0322.4 + 0243
99	rp800471n00	3.3	15.28	10640	1.16	1.17	0.5	C0322.4+0244 N1587,U3063,C0428.1+0033 N1588,U3064,C0428.2+0033
116	$\rm rp900512n00$	3.6	55.20	9034	0.22	2.21	6.6	U03528A,C0642.0+8640
125	wp701047n00	3.4	1.46	9982	1.74	1.03	5.4	U3536A,C0643.0+8638 N2341,U3708,C0706.3+2040 N2342,U3709,C0706.4+2043
136	wp500113	2.6	31.13	4487	0.44	1.38	6.9	C0724.2+1944 C0724.5+1943

Table 4—Continued

(1)	(2)	(3)	(4)	(5)	(6)	(7)	(8)	(9)
137	rp800230n00	3.3	24.10	8782	1.40	1.89	3.6	U3906,C0730.4+7434
								U3906,C0730.4+7437
140	wp200896	3.0	24.71	8046	0.38	1.48	4.7	U3995, C0741.0 + 2921
								U3995, C0741.0 + 2921
144	wp200175	3.4	40.33	8837	0.40	1.48	3.4	U4030, C0745.1 + 2820
								U4030, C0745.1 + 2820
161	rp600542n00	2.8	44.29	2714	0.39	1.78	4.3	I2338,U4383,C0820.7+2130
								I2339,U4383,C0820.7+2130
163	rp701397n00	2.9	43.54	1713	0.74	1.77	4.5	C0825.4 + 5540
								U4427, C0825.3 + 5540
171	rp300203n00	3.3	23.29	4908	-0.24	1.85	3.8	C0843.3 + 1259
								C0843.1 + 1258
175	wp700541	3.8	39.39	6062	1.07	1.58	0.24	N2672,U4619,C0846.5+1916
								N2673,U4620,C0846.5+1916
186	wp800602n00	3.5	12.97	7535	0.45	1.09	3.5	N2750,U4769,C0902.8+2538
								N2750,U4769,C0902.8+2538
200	rp800466n00	3.6	33.74	6624	-1.31	1.42	3.6	C0921.0 + 6447
								C0921.1 + 6445
204	wp701039n00	2.6	36.43	5247	0.65	1.4	3.5	U5044, C0925.0 + 1230
								U5044, C0925.0 + 1230

Table 4—Continued

(1)	(2)	(3)	(4)	(5)	(6)	(7)	(8)	(9)
218	wp600382n00	39.0	19.00	28350	13.1	1.37	20.0	M82,N3034
								U5322,C0951.7+6955
								M81,N3031
								U5318, C0951.4 + 6918
234	rp200076	10.8	53.00	26522	19.30	2.7	3.1	N3226,U5617,C1020.7+2008
								N3227,U5620,C1020.8+2006
238	wp700551	4.3	1.27	4647	34.88	1.0	1.8	C1031.6 + 3953
								C1031.7 + 3954
239	rp300204n00	5.6	23.11	3395	0.65	1.5	6.6	N3286,C1033.1+5853
								N3288,U5752,C1033.2+5849
243	wp800410	3.1	52.75	10748	0.32	2.2	1.6	C1037.8 + 3920
								C1037.8 + 3920
246	rp700384n00	3.8	12.04	9735	0.34	1.12	2.8	C1040.9 + 1222
								C1041.0 + 1221
258	rp700872n00	3.4	35.07	13081	-0.08	1.43	3.7	M159,C1055.4+7253
								C1055.3 + 7254
260	wp300137	3.4	35.60	9395	0.38	1.39	1.3	C1057.0 + 5019
								C1056.9 + 5017
278	rp600263n00	9.5	3.00	23865	4.02	1.05	2.4	N3607,U6297,C1114.3+1819
								N3608,U6299,C1114.4+1825

Table 4—Continued

(1)	(2)	(3)	(4)	(5)	(6)	(7)	(8)	(9)
320	rp600519n00	2.5	31.17	21288	0.09	1.54	1.9	C1203.2+0153
								C1203.2 + 0152
339	rp700346n00	3.2	21.77	7069	-2.74	1.78	2.8	N4447,C1225.7+1410
								N4446,U7586,C1225.6+1441
345	rp800522n00	4.7	51.94	16836	0.06	1.85	1.9	N4521,U7706,C1230.6+6413
								N4512,U7700,C1230.4+6410
347	rp700056n00	5.0	38.24	8990	1.17	1.46	0.10	N4567,U7777,C1234.0+1132
								N4568,U7776,G1234.0+1131
353	rp600017n00	7.5	1.82	13666	14.44	1.02	2.2	N4649,U7898,C1241.1+1150
								N4647,U7896,C1241.0+1152
367	wp201372	3.3	29.75	1710	-2.93	1.82	1.8	I858, U8321, C1312.4 + 1729
								I859,U8320,C1312.5+1729
378	wp800553n00	4.3	14.87	13148	1.13	1.05	3.0	N5183,U8485,C1317.5-0128
								N5184,U8487,C1327.6-0125
402	rp700392n00	3.3	52.00	11095	0.59	2.00	2.0	I960A,U8849,C1353.6+1745
								I960B,U8849,C1353.6+1745
410	rp700345n00	3.1	15.21	7298	0.24	1.11	1.9	N5434,U8965,C1400.9+0941
								U8967,C1401.0+0943
419	rp700332n00	6.8	3.05	4251	4.69	1.03	326.	M1376,N5506,C1410.7-0259
								N5507,C1410.8-0255

Table 4—Continued

(1)	(2)	(3)	(4)	(5)	(6)	(7)	(8)	(9)
422	wp600462	3.4	27.63	14246	0.54	1.34	1.1	N5544,U9142,C1415.0+3648
								N5545,U143,C1415.0+3648
473	rp701373n00	2.6	37.54	15434	0.21	1.48	4.1	U10052,C1547.8+2058
								U10052,C1547.8+2058
494	rp200993	2.9	26.44	3905	20	1.34	1.1	U10325,C1616.0+4613
								U10325,C1616.0+4613
508	wp701080n00	4.1	56.36	16066	0.69	3.05	214.	U10814,C1717.9+4901
								U10814,C1718.0+4905
510	wp701086	2.9	0.79	1922	4.20	1.03	1.5	C1720.7 + 3056
								C1720.7 + 3055
530	wp400043	7.4	24.96	15144	-0.23	1.44	6.0	U1135,C1808.6+3059
	_							N6575,U11138,C1809.0+3105
534	rp800498n00	3.6	50.93	5412	0.18	1.93	5.3	N6621,U11175,C1813.2+6821
	_							N6622,U11175,C1813.2+6820
548	wp500308	3.4	30.66	8690	0.67	1.33	5.7	N6964,U11629,C2044.9+0008
	_							N6962,U11628,C2044.8+0008
557	rp400081	3.1	50.14	8786	0.28	1.95	5.6	U11751,C2126.6+1110
	_							U11751,C2126.6+1110
564	wp700525	5.4	48.01	7409	2.67	1.56	5.5	N7237,U11958,C2122.3+1335
	-							N7236,U11958,C2122.3+1335
<ul><li>510</li><li>530</li><li>534</li><li>548</li><li>557</li></ul>	wp701086 wp400043 rp800498n00 wp500308 rp400081	2.9 7.4 3.6 3.4 3.1	0.79 24.96 50.93 30.66 50.14	1922 15144 5412 8690 8786	4.20 -0.23 0.18 0.67 0.28	1.03 1.44 1.93 1.33 1.95	1.5 6.0 5.3 5.7 5.6	U10814,C1718.0+4905 C1720.7+3056 C1720.7+3055 U1135,C1808.6+3059 N6575,U11138,C1809.0+31 N6621,U11175,C1813.2+68 N6622,U11175,C1813.2+68 N6964,U11629,C2044.9+00 N6962,U11628,C2044.8+00 U11751,C2126.6+1110 U11751,C2126.6+1110 N7237,U11958,C2122.3+13

Table 4—Continued

(1)	(2)	(3)	(4)	(5)	(6)	(7)	(8)	(9)
566	wp701046n00	3.7	0.00	9192	0.02	1.02	6.5	N7253A,U11984,C2217.2+2098
574	rp200986n00	2.9	25.04	3491	0.12	1.21	6.9	N7253B,U11985,C2217.2+2098 U12214,C2248.6+3106 C2248.7+3106

Column (1) - CPG Number

Column (2) - PSPC Sequence Number

Column (3) - Radius of circle

Column (4) - Angle from center of image in arcminutes

Column (5) - Exposure time in seconds

Column (6) - Signal-Noise/3 in PSPC counts/second

Column (7) - Exposure map correction

Column (8) - Column density in  $10^{20}~\rm cm^{-2}$ 

Column (9) - Common galaxy names: (N)GC, (U)GC, (I)C, (C)GCG

TABLE 5
X-RAY SPECTRAL RESULTS

CPG	No. PHA Bins	$\chi^2_{dof}$	Best Fit Temperature (keV)	90% Confidence Range (keV)
99	6	0.36	0.99	0.44 - 64
125	11	0.16	1.09	0.37 - 64
137	6	0.37	0.83	0.06 - 47.
175	6	0.04	0.68	0.27 - 64
218	151	0.48	0.85	0.70 - 1.14
234	162	0.85	2.09	1.67 - 2.73
278	84	33.9	0.40	0.31 - 0.57
347	10	0.33	1.71	0.31 - 64
353	117	0.60	0.82	0.78 - 0.85
378	8	0.11	1.07	0.10 - 64
564	20	0.34	1.03	0.77 - 1.93

Column (5) - the value of  $64~\mathrm{keV}$  is the hard limit imposed by the spectral fitting routine

Table 6
Correlation Test Results: All Pairs

DV	IV	DET/TOT	GKT	Slope	Error	IC	Error
$\log (l_x) (0.25 - 2 \text{ keV})$ $\log (l_x)$	$\log (l_b) \\ \log (l_{FIR})$	$\frac{11/49}{7/36}$	$0.81 \\ 0.40$	0.25	0.49	29.78	_
$\log (l_x) \\ \log (l_x)$	$ \frac{\log (\Delta r)}{\log (\Delta v)} $	11/49 11/49	$0.69 \\ 0.52$	-0.51 -	0.65	40.20	

Table 7
Mean Values of Sample Quantities

Sample	Quantity	Mean	Error
spiral pairs normal spirals early-type pairs normal early-type: $(\log l_x > 43.70)$	$\log (l_x)^a$ $\log (l_x)^b$ $\log (l_x)^c$ $\log (l_x)^d$	40.82 39.87 41.35 42.00	0.11 0.11 0.21 0.13
mixed pairs all pairs compact groups	$\log (\text{obs. } l_x) \stackrel{\text{c}}{=} \log (l_x) \stackrel{\text{e}}{=} \log (l_x) \stackrel{\text{e}}{=}$	40.87 40.86 41.59	0.11 0.09 0.11

 $<sup>^{\</sup>rm a}ROSAT\,\mathrm{PSPC}$  data: extrapolated to 0.5 - 3 keV

 $<sup>^{\</sup>rm b} \emph{EINSTEIN}$  IPC data: 0.5 - 3 keV

 $<sup>^{\</sup>rm c}ROSAT\,{\rm PSPC}$ data: extrapolated 0.2 - 4 keV

 $<sup>^{\</sup>rm d} EINSTEIN\, {\rm IPC}$ data: 0.2 - 4 keV

 $<sup>^{\</sup>rm e}ROSAT\,{\rm PSPC}$ data: 0.25 - 2 keV

TABLE 8
X-RAY SPATIAL RESULTS

CPG	Peak Surface Brightness	$\mathrm{HWHM}(\mathrm{kpc})$	Radial Extent(kpc)
99	3.6	~14	$\sim$ 47
125	24.7	5	17
	15.1	10	25
218	14.5	1	2
	53.4	1	2
234	7.9	15	40
239	13.0	32	74
278	12.6	2	7
	9.2	3	9
353	471.	2	6
564	1.4	80	$\sim 169$

Column (2):  $10^{-3}$  counts  $\sec^{-1}$  cm<sup>-2</sup>

Fig. 1.— Log  $(l_x)$  vs Log  $(l_b)$  is shown for all galaxy pairs. The filled hexagons are detected spiral pairs, the crosses are detected early-type galaxy pairs, the filled triangles are detected mixed pairs, and the open squares are upperlimits for all pair types. Detected pairs with a Seyfert galaxy are represented by an open star. They are shown here but not included in correlations. The X-ray luminosities are given in the 0.25 - 2.0 keV energy band.

Fig. 2.— Log (observed  $l_x$ ) vs Log ( $l_{FIR}$ ) is shown for detections (filled hexagons) and upperlimits (open squares). CPG 419 is detected as has a spiral galaxy. It was shown as a star but not included in the correlations.

Fig. 3.— Log (observed  $l_x$ ) vs Log ( $\Delta r$ ) is shown for detections (filled hexagons) and upperlimits (open squares). Detected pairs with Seyfert galaxies are shown as stars. They are not included in the correlations.

Fig. 4.— Log  $(l_x)$  vs Log  $(l_b)$  is shown for detected spiral galaxy pairs (filled hexagons), normal spiral galaxies (crosses), and spiral pair upperlimits (open hexagons). Pair luminosities are converted to the energy band of the normal galaxies, 0.5 - 3 keV. CPG 419 is detected and has a Seyfert galaxy; it is shown by a star.

Fig. 5.— Log  $(l_x)$  vs Log  $(l_b)$  is shown for detected early-type galaxy pairs (filled hexagons) and detected normal early-type galaxies (filled triangles). The open hexagons are upperlimits for pairs while the open triangles are normal early-type galaxy upperlimits. The pair luminosities are converted to the energy band of the normal galaxies, 0.2 - 4 keV.

Fig. 6.— Log (observed  $l_x$ ) vs Log (predicted

 $l_x$ ) is shown for early-type galaxy pair detections (filled hexagons) and upper limits (open hexagons). Luminosities are converted to 0.2 - 4 keV band.

Fig. 7.— Log (observed  $l_x$ ) vs Log (predicted  $l_x$ ) is shown for mixed galaxy pair detections (filled hexagons) and upperlimits (open hexagons). Luminosities are converted to 0.2 - 4 keV band. CPG 238 and CPG 510 are detected and have Seyfert galaxies; they are shown by a star.

Fig. 8.— Radial profile of CPG 99.

Fig. 9.— Radial profile of CPG 125 on the brightest galaxy.

Fig. 10.— Radial profile of CPG 218 on the brightest galaxy.

Fig. 11.— Radial profile of CPG 234.

Fig. 12.— Radial profile of CPG 239.

Fig. 13.— Radial profile centered on the brightest galaxy in CPG 278.

Fig. 14.— Radial profile of CPG 353.

Fig. 15.— Radial profile of CPG 564.

Fig. 16.— Contour map of CPG 99 is shown for image smoothed with a Gaussian of width 22.5 arcsec. Contour levels are 2 and  $3\sigma$ .

Fig. 17.— Contour map of CPG 234 is shown for image smoothed with a Gaussian of width 22.5 arcsec. Contour levels are 3, 5, and  $10\sigma$ .

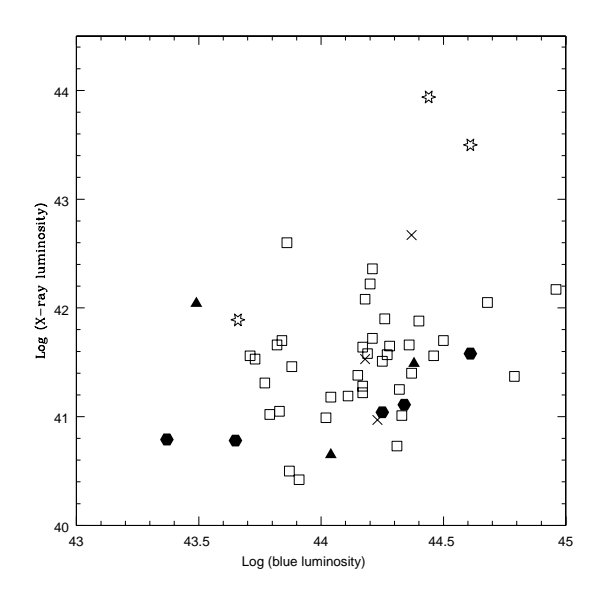
Fig. 18.— Contour map of CPG 239 is shown for image smoothed with a Gaussian of width 22.5 arcsec. Contour levels are 1, 2, and  $3\sigma$ .

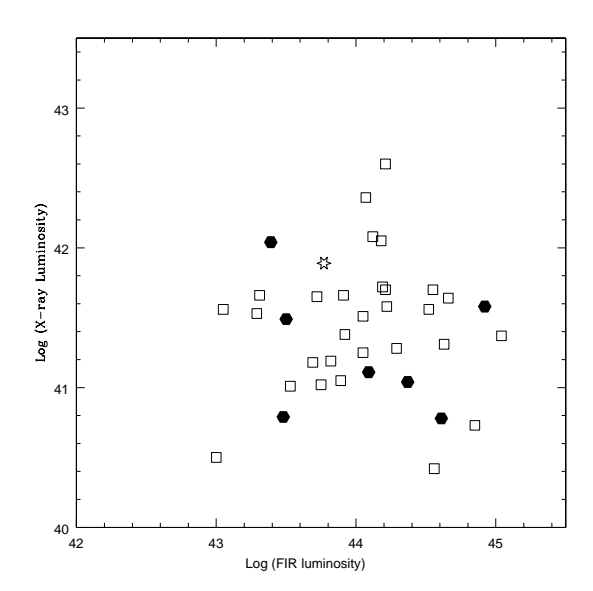
Fig. 19.— Contour map of CPG 278 is shown

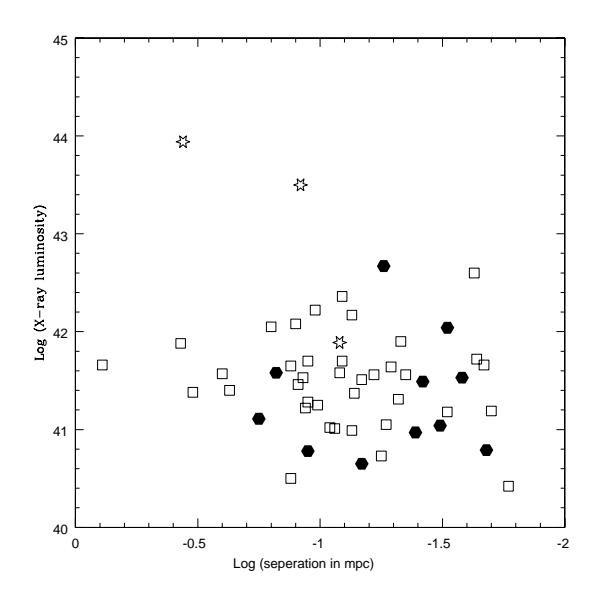
for image smoothed with a Gaussian of width 22.5 arcsec. Contour levels are 3, 5, and  $10\sigma$ .

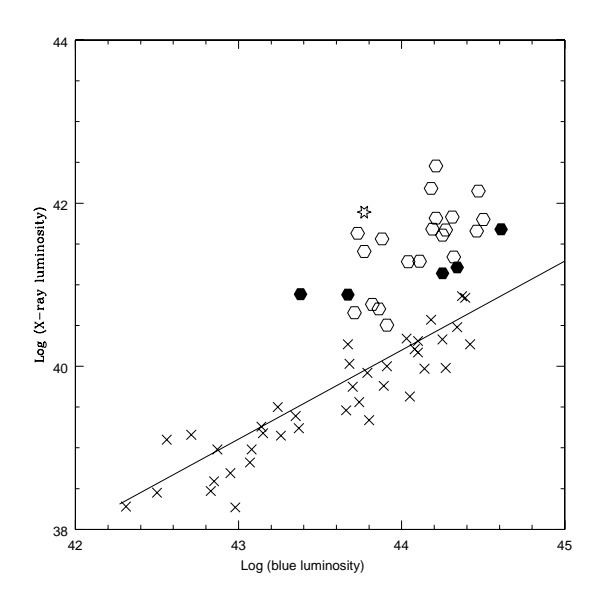
Fig. 20.— Contour map of CPG 353 is shown for image smoothed with a Gaussian of width 22.5 arcsec. Contour levels are 3, 5, 10, 20,  $30, 40\sigma$ .

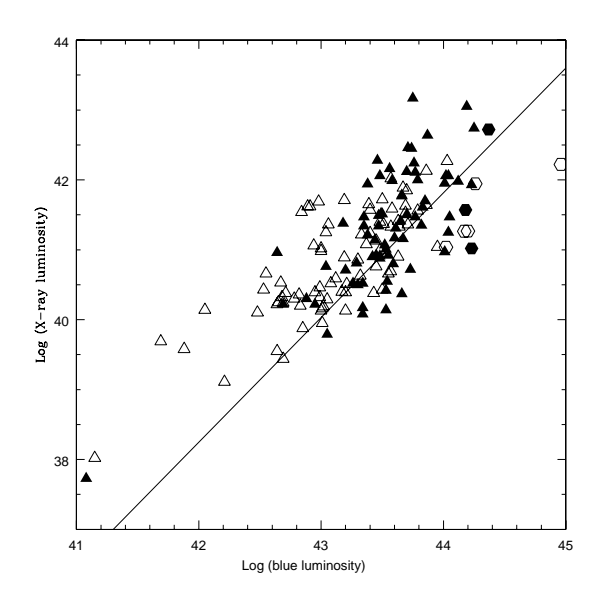
Fig. 21.— Contour map of CPG 564 is shown for image smoothed with a Gaussian of width 22.5 arcsec. Contour levels are 1 and  $2\sigma$ .

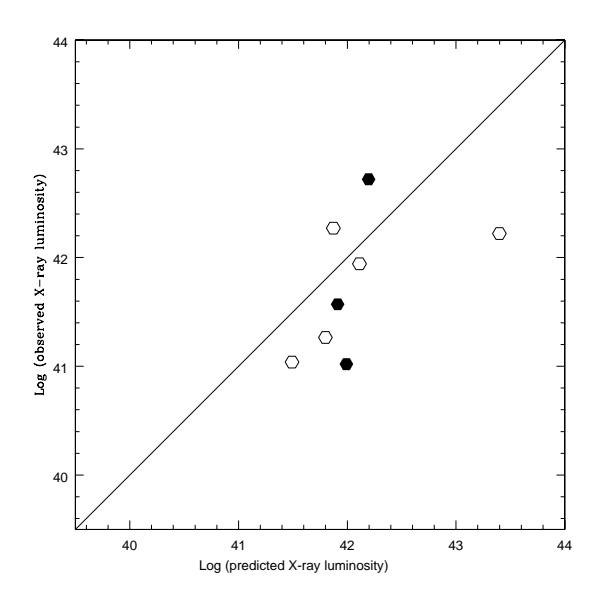


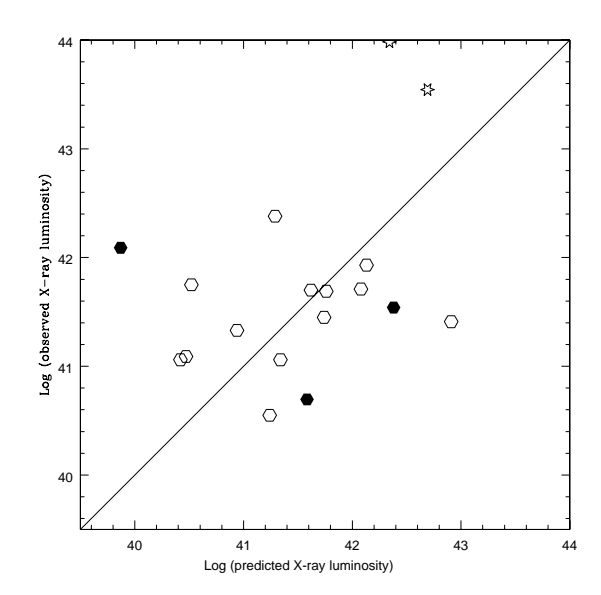


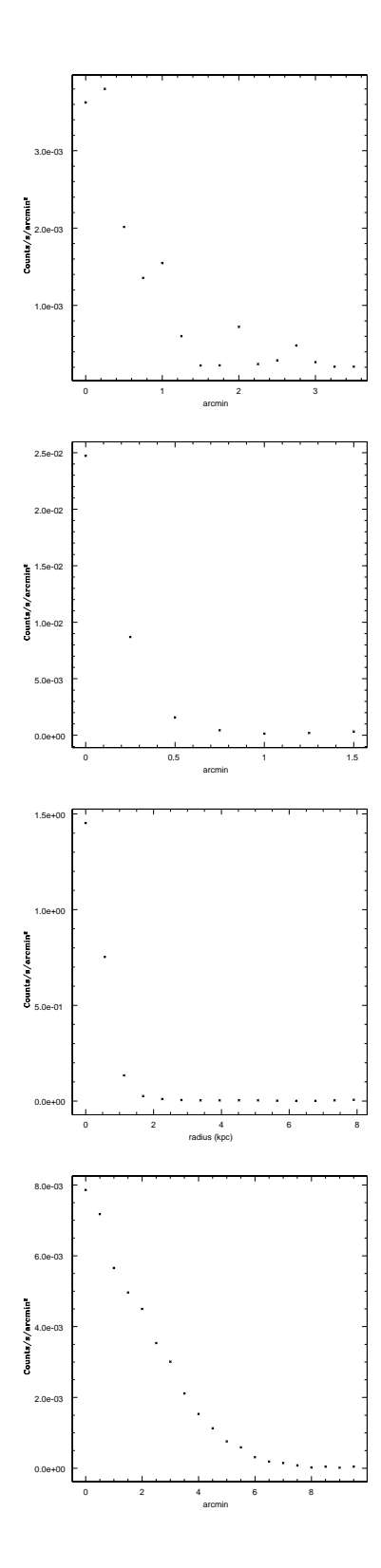


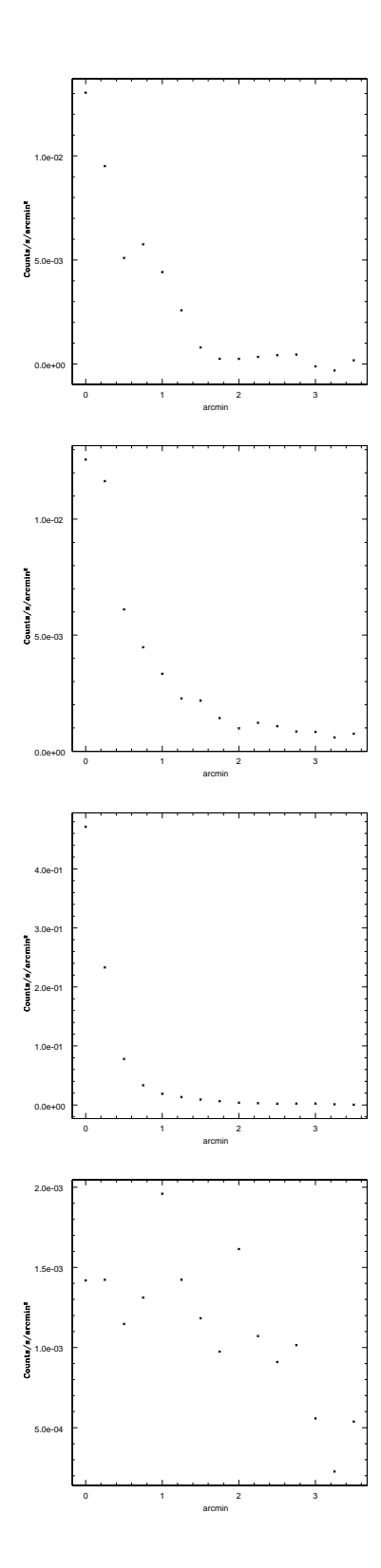












This figure "mh\_16.jpg" is available in "jpg" format from:

This figure "mh\_17.jpg" is available in "jpg" format from:

This figure "mh\_18.jpg" is available in "jpg" format from:

This figure "mh\_19.jpg" is available in "jpg" format from:

This figure "mh\_20.jpg" is available in "jpg" format from:

This figure "mh\_21.jpg" is available in "jpg" format from: